DMD Fast Forward. Published on March 13, 2023 as DOI: 10.1124/dmd.122.000968
This article has not been copyedited and formatted. The final version may differ from this version.

Title Page

Predicting *in vivo* Target Occupancy (TO) Profiles via PBPK-TO Modeling of Warfarin Pharmacokinetics in Blood: Importance of Low Dose Data and Prediction of Stereoselective Target Interactions

Wooin Lee, Min-Soo Kim, Jiyoung Kim, Yasunori Aoki, Yuichi Sugiyama

College of Pharmacy and Research Institute of Pharmaceutical Sciences, Seoul National University, 1 Gwanak-ro, Gwanak-gu, Seoul, 08826, Korea (W.L., M-S.K., J.K.); Laboratory of Quantitative System Pharmacokinetics/Pharmacodynamics, Josai International University, 2-3-11 Hirakawa-cho, Chiyoda-ku, Tokyo 102-0093, Japan (Y.A., Y.S.); Drug Metabolism and Pharmacokinetics, Research and Early Development, Cardiovascular, Renal and Metabolism (CVRM), BioPharmaceuticals R&D, AstraZeneca, Gothenburg, Sweden (Y.A.)

DMD Fast Forward. Published on March 13, 2023 as DOI: 10.1124/dmd.122.000968
This article has not been copyedited and formatted. The final version may differ from this version.

Running title page

Warfarin PBPK modeling with target binding

Correspondence to:
Wooin Lee, Ph.D.
College of Pharmacy and Research Institute of Pharmaceutical Sciences, Seoul National University, 1 Gwanak-ro, Gwanak-gu, Seoul, Korea 08826
Phone: +82-2-880-7873
Fax: +82-2-880-0649
E-mail: wooin.lee@snu.ac.kr

Manuscript metrics:

Number of text pages: 14
Number of tables: 5
Number of figures: 6
Number of references: 28
Number of words in the Abstract: 247 words
Number of words in the Introduction: 748 words
Number of words in the Discussion: 1633 words

Abbreviations:

TMDD, target-mediated drug disposition; PK, pharmacokinetic; PBPK model, physiologically-based pharmacokinetic model; VKOR, vitamin K 2,3-epoxide reductase; OAT2, Organic Anion Transporter 2; ODE, ordinary differential equation; K_p, the tissue-to-blood partitioning coefficients; K_d, the equilibrium dissociation constant; k_a, the absorption rate constant; k_{on}, the association rate constant; k_{off}, the dissociation rate constant; CYP, cytochrome P450; PS, the permeability surface product; V_d, the volume of distribution; CL, clearance; $CL_{int,all}$, the overall intrinsic clearance; X_{TotalR}, the total amount of the receptor; V_{max}, the maximum rate in the Michaelis-Menten equation; CGNM, the Cluster Gauss-Newton Method; SSR, the sum of squared residuals

DMD Fast Forward. Published on March 13, 2023 as DOI: 10.1124/dmd.122.000968
This article has not been copyedited and formatted. The final version may differ from this version.

Abstract

Warfarin is well-recognized for its high-affinity and capacity-limited binding to the pharmacological target and undergoes target-mediated drug disposition (TMDD). Here, we developed a physiologically-based pharmacokinetic (PBPK) model that incorporated saturable target binding and other reported hepatic disposition components of warfarin. The PBPK model parameters were optimized by fitting to the reported blood PK profiles of warfarin with no stereoisomeric separation following oral dosing of racemic warfarin (0.1, 2, 5, or 10 mg) using the Cluster Gauss-Newton Method (CGNM). The CGNM-based analysis yielded multiple "accepted" sets for six optimized parameters, which were then used to simulate the warfarin blood PK and *in vivo* target occupancy (TO) profiles. When further analyses examined the impact of dose selection on uncertainty in parameter estimation by the PBPK modeling, the PK data from 0.1 mg dose (well below target saturation) was important in practically identifying the target binding-related parameters *in vivo*. When stereoselective differences were incorporated for both hepatic disposition and target interactions, our PBPK modeling predicted that R-warfarin (of slower clearance and lower target affinity than S-warfarin) contributes to TO prolongation following oral dosing of racemic warfarin. Our results extend the validity of the approach by which the PBPK-TO modeling of blood PK profiles can yield TO prediction *in vivo* (applicable to the drugs with targets of high affinity and abundance and limited distribution volume via non-target interactions). Our findings support that model-informed dose selection and PBPK-TO modeling may aid in TO and efficacy assessment in preclinical and clinical phase-1 studies.

DMD Fast Forward. Published on March 13, 2023 as DOI: 10.1124/dmd.122.000968
This article has not been copyedited and formatted. The final version may differ from this version.

Significance Statement

The current PBPK modeling incorporated the reported hepatic disposition components and target binding of warfarin and analyzed the blood PK profiles from varying warfarin doses, practically identifying target binding-related parameters *in vivo*. By implementing the stereoselective differences between R- and S-warfarin, our analysis predicted the role of R-warfarin in prolonging overall target occupancy. Our results extend the validity of analyzing blood PK profiles to predict target occupancy *in vivo*, which may guide efficacy assessment in preclinical and clinical phase-1 studies.

DMD Fast Forward. Published on March 13, 2023 as DOI: 10.1124/dmd.122.000968
This article has not been copyedited and formatted. The final version may differ from this version.

Introduction

Target-mediated drug disposition (TMDD) refers to the phenomenon in which the saturable binding of drugs to their pharmacological targets leads to nonlinear pharmacokinetic (PK) behaviors (Levy, 1994). TMDD has been frequently considered for biologics which typically interact with their targets of high specificity and affinity. Once the formation of the drug-target complex reaches saturation with either high doses or repeated dosing, the fraction of the dose binding to the target becomes disproportionately small. As such, systemic drug exposure can increase much larger than expected from a single low dose, leading to dose-dependent PK profiles that are nonlinear at low doses but linear at high doses. Compared to biologics, TMDD occurrence is less common among small-molecule drugs. Yet, TMDD cases have been increasingly reported among small-molecule drugs in recent years (An, 2017).

To enhance our mechanistic understanding of the TMDD among small-molecule drugs, it is important to tease out the relative contribution of saturable target binding to nonlinear PK profiles compared to other components in drug disposition (e.g., saturable metabolism/transport in the liver or intestine). By applying the PBPK modeling with target binding, our group recently reported that target binding, albeit not a major contributor to the nonlinear bosentan PKs, is important in capturing the observed PK profiles at low concentration ranges (Koyama et al., 2021). We also noted that the analysis of blood bosentan PK profiles obtained from a wide range of doses via PBPK modeling with target binding could practically identify target binding-related parameters of bosentan, thereby predicting the target occupancy (TO) profiles *in vivo*. These findings prompted us to pursue additional cases which may expand the validity of our approach of analyzing the blood PK profiles toward the prediction of the TO *in vivo*.

Approved for medical use in 1954, warfarin, a racemic mixture of R- and S-enantiomers, is still considered the mainstay of oral anticoagulant treatment for patients with various cardiovascular diseases. However, the safe use of warfarin remains challenging due to its narrow therapeutic window and large interpatient variability. The anticoagulant effect of warfarin is mediated by high-affinity interactions with its pharmacological target, vitamin K 2,3-epoxide reductase (VKOR), located mainly in the liver. The inhibitory potency of warfarin toward its target varied widely (ranging from nanomolar to millimolar concentrations)

DMD Fast Forward. Published on March 13, 2023 as DOI: 10.1124/dmd.122.000968
This article has not been copyedited and formatted. The final version may differ from this version.

(Bevans et al., 2013), but the underlying reasons for such discrepancies had remained elusive. Later, the presence of dithiothreitol *in vitro* was identified to alter the redox state of VKOR, greatly influencing the inhibitory potencies of warfarin toward VKOR (Shen et al., 2017). The target affinity of warfarin is considered to be stereoselective [S-warfarin being more potent by 3-6 times than R-warfarin, based on the relationship between dose or concentration and response (Breckenridge et al., 1974; O'Reilly, 1974; Hignite et al., 1980)]. Yet, lacking is a detailed understanding of the stereoselective warfarin-target interactions and pharmacological and clinical implications in warfarin therapy.

Saturable target binding of warfarin and its nonlinear PK profiles were noted in rats over four decades ago (Takada and Levy, 1980). Nonlinear PK profiles of warfarin in human subjects, in fact, served as the first case analyzed via TMDD-PK modeling (Levy et al., 2003). Later, a clinical study reported that the saturable target binding of warfarin could hamper the PK extrapolation from a microdose (0.1 mg) to a therapeutic dose (5 mg) (Lappin et al., 2006). The hepatic uptake of warfarin was found to be handled by Organic Anion Transporter 2 (OAT2) with stereoselective affinity and capacity (Bi et al., 2018). So far, none of the previous PK modeling of warfarin incorporated all of the reported components for hepatic warfarin disposition (i.e., metabolism, active uptake, and target binding in the liver). In addition, the previous modeling efforts mainly analyzed the data at therapeutic doses of warfarin but not at a microdose (which displayed a large deviation from dose-proportional PKs).

The current study aimed to develop an updated PBPK-TO model of warfarin by incorporating saturable target binding in addition to the metabolism and uptake components in the liver. Our analysis revisited early clinical data which measured the total warfarin levels from a wide dose range of warfarin, including a microdose. Furthermore, the stereoselective differences between R- and S-warfarin were incorporated in analyzing the warfarin blood PK profiles. We believe that our current results may offer important insights into the factors to consider in predicting and exploiting the TMDD occurrence in small-molecule drug candidates, as well as in designing preclinical studies and clinical phase-1 trials that may shed light on the target engagement *in vivo*.

DMD Fast Forward. Published on March 13, 2023 as DOI: 10.1124/dmd.122.000968
This article has not been copyedited and formatted. The final version may differ from this version.

Materials and Methods

Structure of the warfarin PBPK model

Our PBPK model for warfarin was constructed based on *in silico, in vitro*, and clinical PK data available from the literature. As depicted in Figure 1, the PBPK model included the central (blood) compartment connected to the liver, subdivided into five extrahepatic and hepatocellular compartments, and incorporated the active uptake and target binding components for warfarin. The structure of our PBPK model was similar to that reported previously, except for having the target binding components in the hepatocellular compartments (Koyama et al., 2021). To accommodate the large volume of distribution observed with warfarin, the central (blood) compartment was connected to three large-volume tissues (adipose, muscle, and skin) with the assumption of rapid equilibrium and using the tissue-to-blood partitioning coefficients (K_p) calculated *in silico* using the method reported by Rodgers and Rowland (Rodgers and Rowland, 2006). Orally administered warfarin was assumed to be completely absorbed from the intestine to the extrahepatic compartment with a first-order rate constant k_a (/h), similar to the previous report (Bi et al., 2018). The hepatic disposition processes of warfarin were described by incorporating the following components: active influx by OAT2, metabolism by cytochrome P450 (CYP) enzymes, and target binding to VKOR.

Our PBPK model was fitted to the reported average blood PK profiles of warfarin with no stereoisomeric separation [2, 5, and 10 mg (King et al., 1995); 0.1 mg (Lappin et al., 2006)] (Figure 2A). The analysis included no interindividual variability as we had no access to individual-level data. Initially, the modeling was done using ordinary differential equations (ODEs) which did not separate R- and S-warfarin. The model included a total of 24 parameters, including six unknown and 18 fixed parameters (Table 1). Subsequent analyses <RS#1-#3> utilized the same reported blood PK dataset, but the ODEs were separated for R- and S-warfarin. Stereoselective parameters were estimated from the information available in the literature. The model included a total of 26 parameters, including six unknown (4 stereoselective parameters; X_{TotalR} and k_a kept the same for R- and S-warfarin) and 20 fixed parameters (Table 2).

DMD Fast Forward. Published on March 13, 2023 as DOI: 10.1124/dmd.122.000968
This article has not been copyedited and formatted. The final version may differ from this version.

Parameters for the warfarin PBPK model

The hepatic permeability clearance of warfarin was considered by incorporating the active influx clearance mediated mainly by OAT2 ($PS_{act,inf}$ described using $V_{max(act,inf)}$ and $K_{m(act,inf)}$) along with the permeability clearance via passive influx and efflux ($PS_{dif,inf,}$ and $PS_{dif,eff}$, respectively). The experimentally measured $K_{m(act,inf)}$ values for R- and S-warfarin were reported to be 7.3 and 10.4 μM, respectively (Bi et al., 2018). The same study reported the $V_{max(act,inf)}$ and $PS_{dif,inf}$ values (per million hepatocytes), yielding the corresponding values of 3,063 μmole/h and 12.0 L/h for an adult of 70 kg body weight (the following scaling factors were used; 118 million hepatocytes/g liver; 24.5 g liver/kg body weight). For the initial model fitting of the warfarin PK profiles, $V_{max(act,inf)}$ was set as unknown (the lower and upper ranges set as 10^{-2} and 10^{2}-fold to the base value 3,063 μmole/h), and $K_{m(act,inf)}$ was fixed as 8.85 μM (Table 1). Subsequent analyses <RS#1-#3> considered the stereoselective differences for $K_{m(act,inf)}$ (fixed as 7.3 and 10.4 μM for R- and S-warfarin, respectively) and $V_{max(act,inf)}$ [optimized for R-warfarin; the reported fold-difference of 0.506 was then used to calculate the corresponding value for S-warfarin, (Bi et al., 2018)] (Table 2).

The intrinsic metabolic clearance ($CL_{int(met)}$) of warfarin in the hepatocellular compartment was described using $V_{max(met)}$ and $K_{m(met)}$. For the model fitting of the warfarin PK profiles, $K_{m(met)}$ was fixed as 10 μM considering the reported $K_{m(met)}$ values ranging from 3.9 to 24.3 μM (Shaik et al., 2016). The previous study reported the $CL_{int(met)}$ values of 0.1175 and 0.365 μmol/min/mg microsomal protein for R- and S-warfarin, respectively (Bi et al., 2018). By applying the scaling factors (40 mg microsomal proteins/g liver; 24.5 g liver/kg body weight) and using the assumed $K_{m(met)}$ value (10 μM), the $V_{max(met)}$ values were estimated as 4.145 and 12.88 L/h for R- and S-warfarin, respectively. For the initial model fitting of the warfarin PK profiles, $V_{max(met)}$ was set as unknown (the lower and upper ranges set as 10^{-2} and 10^{2}-fold to the base value 8.511 μmole/h) (Table 1). Subsequent analyses <RS#1-#3> considered the stereoselective differences for $V_{max(met)}$ [optimized for R-warfarin; the reported fold-difference of 3.10 was used to calculate the corresponding value for S-warfarin (Bi et al., 2018)] (Table 2).

DMD Fast Forward. Published on March 13, 2023 as DOI: 10.1124/dmd.122.000968
This article has not been copyedited and formatted. The final version may differ from this version.

The target binding of warfarin was modeled to be connected to the hepatocellular compartment [reflecting the primary location of VKOR inside hepatocytes (Hazelett and Preusch, 1988)] with the assumption that warfarin binds reversibly to VKOR in the stoichiometric ratio of 1:1 with the dissociation rate constant k_{off} and the equilibrium dissociation constant K_d (the association rate constant k_{on} was defined automatically as k_{off}/K_d). For the initial model fitting of the warfarin PK profiles, the parameters of k_{off}, K_d, and X_{TotalR} were set as unknown parameters [with the base values based on the previous report (Levy et al., 2003); Table 1] using the following Eqs. (1) and (2):

$$\frac{dX_{FreeR(i)}}{dt} = k_{off} \cdot X_{RDcomplex(i)} - \frac{k_{off}}{K_d} \cdot f_h \cdot C_{HC(i)} \cdot X_{FreeR(i)} \qquad \text{Eq. (1)}$$

$$\frac{dX_{RDcomplex(i)}}{dt} = \frac{k_{off}}{K_d} \cdot f_h \cdot C_{HC(i)} \cdot X_{FreeR(i)} - k_{off} \cdot X_{RDcomplex(i)} \qquad \text{Eq. (2)}$$

$$\text{(Initial conditions at time zero, } X_{FreeR(i)}(0) = X_{TotalR}/5, X_{RDcomplex(i)}(0) = 0)$$

($X_{FreeR(i)}$, $X_{RDcomplex(i)}$, and $X_{TotalR(i)}$ represent the amounts of free target, drug-target complex, and total target in the *i*th hepatocellular compartment, respectively; f_h and $C_{HC(i)}$ represent the fraction of unbound warfarin and the total concentration of warfarin in the *i*th hepatocellular compartment, respectively).

Subsequent analysis <RS#1-#3> utilized the ODEs separated for R- and S-warfarin except for Eq. (3), which was revised from Eq. (1) to consider the competitive interactions of S- and R-warfarin for the free target:

$$\frac{dX_{FreeR(i)}}{dt} = k_{off} \cdot (X_{RDcomplex(i),R-warfarin} + X_{RDcomplex(i),S-warfarin}) - \frac{k_{off}}{K_d} \cdot f_h \cdot (C_{HC(i),R-warfarin} + C_{HC(i),S-warfarin}) \cdot X_{FreeR(i)} \qquad \text{Eq. (3).}$$

$$\text{(Initial condition at time zero, } X_{FreeR(i)}(0) = X_{TotalR}/5)$$

($X_{RDcomplex(i),R\text{-}warfarin}$ and $X_{RDcomplex(i),S\text{-}warfarin}$ represent the amounts of drug-target complex by the respective R- and S-isomers in the *i*th hepatocellular compartment; $C_{HC(i),R\text{-}warfarin}$ and $C_{HC(i),S\text{-}warfarin}$ represent the total concentration of R- and S-warfarin in the *i*th hepatocellular compartment, respectively).

The analyses of <RS#2> and <RS#3> incorporated S-warfarin having the K_d value three-fold lower than R-warfarin, but assumed the stereoselective differences at the association and dissociation steps, respectively (Table 2).

DMD Fast Forward. Published on March 13, 2023 as DOI: 10.1124/dmd.122.000968
This article has not been copyedited and formatted. The final version may differ from this version.

Parameter Optimization by the Cluster Gauss-Newton Method (CGNM)

Being computationally efficient and robust in obtaining multiple possible solutions to nonlinear least-square problems, the Cluster Gauss-Newton method (CGNM) has been recently applied to the PBPK modeling of bosentan (Koyama et al., 2021) and CP-1 (Mochizuki et al., 2022; Yoshikado et al., 2022). A key assumption of the CGNM is that for some model parameters not identifiable from the data, multiple parameter combinations may provide equally as good model fits as the best model fit. Briefly, the CGNM finds multiple best-fit parameter combinations by repeating the parameter estimations from a wide range of initial iterates. Our initial analysis with the ODEs of no stereoisomeric separation uniformly and randomly generated 1,000 initial combinations of 6 unknown parameters (K_d, k_{off}, X_{TotalR}, k_a, $V_{max(met)}$, and $V_{max(act,inf)}$) with user-specified upper and lower ranges (typically, 10^{-2} to 10^2-fold to the base values; Table 1). Then using each of these parameter combinations as the initial iterate, the parameter combination was iteratively moved until it reached the minimum sum of squared residuals (SSR) as defined below:

$$\mathrm{SSR} = \sum_{i=1}^{n}\left(\log_{10} y_{obs,i} - \log_{10} y_{model-predicted,i}\right)^2 \qquad \text{Eq. (4)}$$

($y_{obs,i}$, the ith observed value; $y_{model\text{-}predicted,i}$, the ith model-predicted value)

As the above-mentioned approach using a conventional nonlinear least squares algorithm (e.g., Gauss-Newton method) is computationally intensive, the CGNM was made to remedy the computational bottleneck [see (Aoki et al., 2020) for detailed comparison with conventional algorithms].

The PBPK modeling was done by numerically integrating a set of ODEs by RxODE version 1.1.2 with default setting (Fidler M, 2022) and the CGNM implemented in R version 4.0.3, CGNM package version 0.3.1 (Aoki, 2022) with default setting except having a set number of initial parameter combinations (num_minimizersToFind) to 1,000 and the number of iteration (num_iteration) to 100 as suggested in the user manual. To select parameter combinations from final iterates with similarly small SSR values, the SSR values from parameter combinations were plotted in ascending order. In theory, we wish to find parameter combinations with identical minimum SSR values. However, in reality, it is often not possible with numerical artifacts. Thus, we used a heuristic called the “elbow method” to detect a sudden increase in SSR. Before we

DMD Fast Forward. Published on March 13, 2023 as DOI: 10.1124/dmd.122.000968
This article has not been copyedited and formatted. The final version may differ from this version.

applied the elbow method, we rejected parameter combinations that were statistically significantly worse than the minimum SSR by assuming chai square distribution of SSR (with cutoff alpha 0.05). If there were multiple sudden increases in SSR, the elbow method may not find the first sudden increase. In that case, the elbow method was repeated until similarly small SSRs were selected. The analysis was conducted using acceptedApproximateMinimizers command in the CGNM package and the resulting selections of parameter combinations were referred to as "accepted."

Parameter estimation uncertainty quantification by the bootstrap analysis

To quantify the parameter estimation uncertainty, residual resampling bootstrap analyses were conducted by creating 200 bootstrap datasets and re-estimating the parameters. Each re-estimation was conducted from an initial iterate randomly selected from the accepted parameter combinations. This analysis was conducted using Cluster_Gauss_Newton_Bootstrap_method command in CGNM package and the parameter distributions obtained from the bootstrap analysis were plotted as histograms.

***Post hoc* study design evaluation to assess the importance of dose selection for the estimation of target binding-related parameters**

To assess how the study design, in terms of dose selection, can impact the estimation of target binding-related parameters (K_d, k_{off}, and X_{TotalR}), we investigated their estimation uncertainties with varying three-dose-level designs. The following designs were created by removing one dose arm from the full dataset: <design A> contains 2, 5, and 10 mg arms; <design B> contains 0.1, 5, and 10 mg arms; <design C> contains 0.1, 2, and 5 mg arms; <design D> contains 0.1, 2, and 10 mg arms. CGNM was used to obtain accepted parameter combinations for each dataset, and then the bootstrap analyses were conducted for K_d, k_{off}, X_{TotalR} for each dataset.

DMD Fast Forward. Published on March 13, 2023 as DOI: 10.1124/dmd.122.000968
This article has not been copyedited and formatted. The final version may differ from this version.

Results

CGNM-based parameter optimization for warfarin PBPK modeling and prediction of TO profiles

Our PBPK-TO modeling analyzed the reported nonlinear PK profiles of warfarin over 120 h at four warfarin dose levels (0.1, 2, 5, and 10 mg) (Figure 2A). The "accepted" parameter sets (determined by the elbow method described in the Methods section) showed nearly identical SSR values of around 0.115 (Table 3). When the CGNM runs were repeated two additional times with different initial iterates, the results were nearly identical (Table S1). Five out of six optimized parameters were distributed in a very tight range, with the "rank 1" parameter values (with the smallest SSR) and median values nearly identical. The exception was for $V_{max(act,inf)}$, which varied widely among the accepted parameter sets. Similar to our previous study of bosentan (Koyama et al., 2021), the CGNM-based PBPK modeling of the blood warfarin PK profiles alone appeared to achieve practical identifiability for three parameters related to the target binding *in vivo* (K_d, k_{off}, and X_{TotalR}).

For all four dose levels, the accepted parameter sets well captured the observed blood PK profiles and predicted the TO profiles in a narrow range for each dose level (Figure 2). Despite a wide variation in the $V_{max(act,inf)}$ values among the 663 sets of the accepted parameters, the accepted parameter sets yielded overlapping blood PK profiles, which appeared nearly as a single profile for each dose level (Figure 2A). Such good agreements could be explained by the calculation results showing nearly identical values of 11.93 L/h for the overall intrinsic clearance ($CL_{int,all}$ based on the extended clearance concept model) despite a wide variation in the $V_{max(act,inf)}$ values (Table 3). These results support that the active uptake is unlikely to be rate-determining in the overall hepatic elimination of warfarin. The 633 sets of the accepted parameter combinations also led to the simulated TO profiles, which appeared nearly as a single profile for each dose level (Figure 2B). The ranges of the accepted parameters were very narrow with the rank 1 and median values nearly identical. As an example, the rank 1 parameter combinations were used to simulate the TO profiles. The maximum TO values of 0.064, 0.818, 0.952, and 0.980 for 0.1, 2, 5, and 10 mg, respectively. The predicted TO values at 120 h post-dosing were 0.050, 0.574, 0.757, and 0.859 for 0.1, 2, 5, and 10 mg, respectively.

DMD Fast Forward. Published on March 13, 2023 as DOI: 10.1124/dmd.122.000968
This article has not been copyedited and formatted. The final version may differ from this version.

Impact of dose selection on prediction of warfarin TO profiles via PBPK-TO modeling

To examine whether and how much dose selection impacts parameter estimation and TO prediction from the blood PK data, the CGNM results were compared using four study designs of three-dose-level combinations. Similar to <ALL dataset (0.1, 2, 5, and 10 mg)>, all four study designs <designs A to D> well captured the observed blood PK profiles (Figure 3A) and predicted the TO profiles in a tight range (Figure 3B). <Design A> omitting the dose of 0.1 mg yielded the rank 1 parameter values comparable to those from <ALL dataset>, except for k_{off} (0.0903 vs 0.0432 /h; 2.1-fold differences) and $V_{max(act,inf)}$ (Table 4, Figure 4A). The ranges of the final parameters were very narrow, yielding nearly identical values for the rank 1 and median values. The rank 1 parameter k_{off} value (0.0432 /h) from <design A> was comparable to the reported k_{off} value (0.0405 /h) from the previous TMDD-PK modeling which had analyzed the 2, 5, and 10 mg doses (Levy et al., 2003). For <designs B, C, and D>, which included 0.1 mg data, the accepted parameters also well captured the observed blood PK profiles of warfarin and predicted the TO profiles in a tight range (Figure 3). Unlike <design A>, the rank 1 parameter values for k_{off} was comparable between <designs B, C, and D> and <ALL dataset>: 0.0961, 0.932, 0.0901 vs. 0.0903 /h (Table 4). The bootstrap analysis informed that <design A> was associated with greater uncertainty in parameter estimation, noticeably, for the two parameters related to the target binding (K_d and k_{off}) (Figure 4B). Compared to <design A>, the uncertainty in parameter estimation was reduced to some extent in <design B> and to a greater extent in <designs C and D> which included both 0.1 and 2 mg, noticeable for X_{TotalR} (Figure 4B).

Warfarin PBPK-TO modeling incorporating stereoselective differences and prediction of TO profiles by individual stereoisomers

For the scenario of <RS#1> (with stereoselective consideration in the hepatic metabolism and uptake processes but not in target interactions), the accepted parameter sets well captured the reported blood PK profiles of warfarin (measured with no stereoisomeric separation) at all four dose levels (sold black lines, Figure 5A). The predicted blood PK profiles for S-warfarin declined more rapidly than those for R-warfarin, in line with the calculated $CL_{int,all}$ values of 20.7 and 7.29 L/h for S- and R-warfarin, respectively (Table 5). At the dose levels of 0.1 and 2 mg, the simulated TO profiles for S- and R-warfarin decreased over 120 h, with a more rapid decline for S-warfarin than R-warfarin (Figure 5A). At the dose levels of 5 and 10 mg, the

DMD Fast Forward. Published on March 13, 2023 as DOI: 10.1124/dmd.122.000968
This article has not been copyedited and formatted. The final version may differ from this version.

TO profiles by S-warfarin declined steadily, but those by R-warfarin increased over time, attributable to the increasing engagement of R-warfarin to the target that became available from the dissociation of the target complexed with S-warfarin (Figure 5A).

The scenarios of <RS#2> and <RS#3> assumed three-fold differences in the target affinity (K_d) between R- and S-warfarin (S-warfarin having a 3-fold lower K_d value than R-warfarin) arising from the differences at the association and dissociation steps, respectively. In either scenario, the PBPK models captured the reported blood PK profiles of warfarin with the accepted SSR comparable to those of <RS#1> (Figures 5B and 5C, Table 5). For <RS#2> (S-warfarin with three-fold greater k_{on} than R-warfarin), the simulation results showed that at early time points, the target engagement was dominated by S-warfarin over R-warfarin: At 2 h post-dosing, the target engagement by S-warfarin was greater by 1.56-, 1.93-, 2.29- and 2.46-fold than by R-warfarin at the 0.1, 2, 5, and 10 mg dose levels, respectively (Figure 5B). However, the target engagement by R-warfarin was predicted to be dominant from approximately 60 h post-dosing on (Figure 5B, appearing as cross-over points in the simulated TO profiles). Different from <RS#2>, the results from <RS#3> (S-warfarin assumed to have one-third k_{off} to R-warfarin) predicted the target engagement comparable between R- and S-warfarin at early time points, especially within 1 h post-dosing (Figure 5C). The target engagement by S-warfarin stayed dominant over R-warfarin until the cross-over points at approximately 60 h post-dosing (Figure 5C).

DMD Fast Forward. Published on March 13, 2023 as DOI: 10.1124/dmd.122.000968
This article has not been copyedited and formatted. The final version may differ from this version.

Discussion

The current study developed a PBPK-TO model that can analyze the systemic warfarin PK profiles and predict TO profiles *in vivo*. Like the case of bosentan (Koyama et al., 2021), the CGNM-based analysis of the systemic warfarin PK profiles alone yielded practically identifiable target binding parameters and predicted TO profiles in a very tight range (Table 3, Figure 2). Further analyses indicated that dose selection (the inclusion of 0.1 mg dose; which leads to systemic drug exposure well below target saturation) is important in reducing the uncertainty in estimating target binding-related parameters (Figure 4, Table 4). By incorporating the stereoselective differences between R- and S-warfarin, the current PBPK-TO model predicted the target engagement of each stereoisomer under differing scenarios (Figure 5). Overall, these findings extend the validity of the approach by which the mechanistic PBPK-TO modeling captures the impact of saturable target binding on the systemic PK data and, in turn, allows for the identification of target binding parameters (thereby, TO profiles *in vivo*) based on the systemic PK data alone.

In developing the current PBPK-TO model, the two previous reports on warfarin PK modeling provided a key foundation (Levy et al., 2003; Bi et al., 2018). Bi et al. (Bi et al., 2018) provided the estimates for various parameters of the PBPK model including the handling of warfarin by OAT2. The authors reported that the active uptake of warfarin mediated by OAT2 contributes to the inter-patient variability (Bi et al., 2018). Those results are not contradictory to those from our current study, in that the inter-patient variability of $CL_{int,all}$ may be impacted by both $PS_{act,inf}$ and $CL_{met,int}$ (shown in Eq. (*2), Table 3 footnote). If one compares, regarding their relative contribution to inter-patient variability associated with $CL_{int,all}$, $CL_{met,int}$ is likely to have a greater contribution than $PS_{act,inf}$ which has additional terms of γ and $PS_{dif,inf}$ in Eq. (*2). Different from the previous TMDD modeling of warfarin based on the compartmental model with the target binding component connected to the central component (Levy et al., 2003), our current PBPK-TO model incorporated target binding connected to the hepatocellular compartment (reflecting the primary location of VKOR in hepatocytes) (Figure 1). During CGNM-based parameter optimization in our current study, the initial parameter sets were randomly selected from the ranges covering 10^{-2}- to 10^{2}-fold to the base values from the previous reports (Tables 1 and 2). Despite having four orders of magnitude ranges in which initial iterates could be selected,

DMD Fast Forward. Published on March 13, 2023 as DOI: 10.1124/dmd.122.000968
This article has not been copyedited and formatted. The final version may differ from this version.

our analysis with the ODEs of no stereoisomeric separation yielded the final optimized parameters for target binding *in vivo* in a tight range indicating these parameters are identifiable from the plasma concentration data: the rank 1 and median parameter values were nearly identical, being 6.30 nM, 0.0903 /h, and 4.26 μmole for K_d, k_{off}, and X_{TotalR}, respectively (Table 3). In the literature, the K_d values for the binding of warfarin to VKOR vary widely, attributable in part to the differences in *in vitro* binding assay conditions (in particular, the presence of reducing agents altering the redox state of VKOR) (Bevans et al., 2013; Shen et al., 2017). Our current study supports the predictive utility of the PBPK-TO modeling for *in vivo* target binding parameters when the blood PK profiles are available with appropriate dose selection.

The model-predicted target abundance (X_{TotalR}) for warfarin was 4.26 μmole for 70 kg human body (Table 3). For warfarin doses of 0.1 and 2 mg (corresponding to 0.325 and 6.49 μmole, respectively), the high-affinity interaction of the drug with the target (X_{TotalR} of 4.26 μmole) may represent a significant fraction of the doses. The binding mode of warfarin to VKOR is not fully understood, and some controversies still exist as to whether or not the binding is reversible (Wu et al., 2018). When the formation of the warfarin-target complex is assumed to be reversible (thus not serving as a clearance mechanism), the high-affinity interactions between warfarin and its target may still impact the volume of distribution (V_d) by providing additional drug distribution space to which the drug initially and preferentially distributes. The V_d values calculated using non-compartmental analysis confirm such a nonlinear relationship for the blood PK dataset analyzed in the current study (Figure 6A). In theory, at a very low dose, the apparent V_d would approximate the summation of X_{TotalR}/K_d and V_d via non-specific (non-target-mediated) tissue binding, $V_{d(non\text{-}target)}$, as illustrated in Figure 6B. With escalating doses, the high-affinity target binding becomes saturated and no longer contributes to apparent drug distribution space (thus approximating $V_{d(non\text{-}target)}$). In the case of warfarin and other drugs with targets of high affinity and abundance (i.e., small K_d and large X_{TotalR}) and limited distribution via non-specific tissue binding (i.e., small $V_{d(non\text{-}target)}$), the substantial contribution of X_{TotalR}/K_d to the V_d can be expected, noticeable especially at low doses. For highly lipophilic drugs with less confined tissue distribution (i.e., large $V_{d(non\text{-}target)}$), the impact of target binding would be minimal or not readily discernible (Figure 6B). For small-molecule drugs which feature large X_{TotalR}/K_d and small $V_{d(non\text{-}target)}$ values, it can be postulated that the PK

DMD Fast Forward. Published on March 13, 2023 as DOI: 10.1124/dmd.122.000968
This article has not been copyedited and formatted. The final version may differ from this version.

data at low doses, including a microdose, can provide valuable information in ascertaining the ratio of X_{TotalR}/K_d. When the dose ranges cover from low (well below target saturation; informative on X_{TotalR}/K_d) and high doses (at target saturation; informative on $V_{d(non\text{-}target)}$), the analysis of the systemic PK data alone may allow for the prediction of TO with reasonable certainty.

Our current results using warfarin imply a potentially important yet under-appreciated advantage that the PBPK modeling and microdosing approach may offer for the development of small-molecule drug candidates with potential for TMDD (Burt et al., 2020). If a drug candidate is predicted to have a significant contribution to the target binding-related component (i.e., large X_{TotalR}/K_d and relatively small $V_{d(non\text{-}target)}$), our proposal is to verify the *in vivo* occurrence of the TMDD in preclinical animals by obtaining the blood PK data with ascending doses including a microdose, and intermediate and high doses (covering varying degrees of target binding). In the case of warfarin, the blood PK data in rats clearly indicated much larger V_d values in those receiving 0.1 mg/kg than those receiving 1 mg/kg (Takada and Levy, 1980). With appropriate consideration of the species differences in the target binding-related parameters (e.g., X_{TotalR}, K_d, unbound fraction), it may be possible to identify drug candidates with a high likelihood of TMDD in humans. In such cases, the blood PK data from a microdosing study and PBPK-TO modeling can provide invaluable insights into TO profiles *in vivo*, potentially guiding the interpretation and optimization of pharmacodynamic responses in humans. The prospect of obtaining the TO profiles *in vivo* from the blood PK data alone may aid in overcoming the difficulties in translating *in vitro* potency to *in vivo* efficacy.

By incorporating the stereoselective differences in hepatic disposition and target binding between R- and S-warfarin, the current PBPK-TO model analyzed the blood PK profiles of warfarin (measured with no stereoisomeric separation) and predicted the TO profiles by individual stereoisomers under differing scenarios. Both <RS#2> and <RS#3> shared the assumption that S-warfarin has a 3-fold higher affinity than R-warfarin (i.e., $K_{d,S\text{-}warfarin}$ being one-third to $K_{d,R\text{-}warfarin}$) based on the information available in the literature (Breckenridge et al., 1974; O'Reilly, 1974; Hignite et al., 1980). While <RS#2> assumed that K_d differences arise from the association process (i.e., $k_{on,S\text{-}warfarin}$ being three times to $k_{on,R\text{-}warfarin}$), <RS#3> assumed that K_d

DMD Fast Forward. Published on March 13, 2023 as DOI: 10.1124/dmd.122.000968
This article has not been copyedited and formatted. The final version may differ from this version.

differences arise from the dissociation process (i.e., $k_{off,S\text{-}warfarin}$ being one-third to $k_{off,R\text{-}warfarin}$). Currently, there is no data that experimentally verified the stereoselective differences in the binding affinity of R- and S-warfarin. Of note, Cheng et al. {Cheng, 2023 #626} applied the PK modeling with the TMDD components to the observed plasma PK profiles of S- and R-warfarin independently. The results showed 3.61-fold differences in the K_d values of S- and R-warfarin (in line with the assumption of 3-fold K_d differences in our current study). Molecular docking simulation predicted energetically favorable interactions for S-warfarin than for R-warfarin in binding with human VKOR (Lewis et al., 2016). Yet, it remains to be verified whether the stereoselective differences between S- and R-warfarin in interacting with VKOR involve association, dissociation, or both. In our analysis, the TO profiles by individual stereoisomers showed some differences between <RS#2> and <RS#3> (Figure 5). However, between <RS#2> and <RS#3>, little differences were observed in the *summed* TO profiles by R- and S-warfarin. These results may be explained by the compensatory, competitive formation of the drug-target complex between R- and S-warfarin. For instance, S-warfarin is more rapidly cleared than R-warfarin, and the equilibrium gets shifted toward the dissociation of the S-warfarin-target complex, and the dissociated target would become available to complex with R-warfarin. When the TO profiles were simulated for a typical repeated warfarin dosing regimen (10 mg for 2 days and 3 mg afterwards), the results also showed a similar profile of the compensatory formation of R-warfarin-target complex (Figure S1). As such, the dosing of racemic warfarin may prolong the target engagement and produce the target engagement and pharmacodynamic effect with a lesser degree of inter- and intra-individual variability than the dosing of single stereoisomeric warfarin.

In conclusion, we successfully developed and applied an updated PBPK-TO model to analyze the blood PK profiles of warfarin over a wide dose range, including a microdose. Our results using warfarin support the approach by which target engagement *in vivo* may be predicted with reasonable certainty from the analysis of the systemic PK data impacted by target binding. Opportunity for prediction of target engagement *in vivo* may be attainable with the model-informed selection of a dose range covering a varying extent of target saturation, in particular, by including low doses below target saturation during dose escalation of clinical phase-1 trials. Information obtained on target engagement *in vivo* can serve as a valuable guide and tool in interpreting and optimizing pharmacodynamic responses.

DMD Fast Forward. Published on March 13, 2023 as DOI: 10.1124/dmd.122.000968
This article has not been copyedited and formatted. The final version may differ from this version.

Acknowledgements

The authors would like to thank Satoshi Koyama and Kota Toshimoto (Astellas Pharma Inc) for the support in conducting the initial PBPK modeling. Byung Woo Han, Jin Mo Kang (Seoul National University) and Sangwook Wu (Pukyong National University) are acknowledged for their helpful discussion regarding the interpretation and prediction of the target binding kinetics of warfarin.

Data Availability Statement

The authors declare that all the data supporting the findings of this study are contained within the paper.

Authorship contributions

Participated in research design: WL, YA, YS

Performed data analysis: MK, WL, JK, YA, YS

Wrote or contributed to the writing of the manuscript: WL, MK, JK, YA, YS

References

An G (2017) Small-Molecule Compounds Exhibiting Target-Mediated Drug Disposition (TMDD): A Minireview. *J Clin Pharmacol* **57:**137-150.

Aoki Y (2022) CGNM: Cluster Gauss-Newton method. R package version 0.3.1.

Aoki Y, Hayami K, Toshimoto K, and Sugiyama Y (2020) Cluster Gauss–Newton method. *Optimization and Engineering*.

Bevans CG, Krettler C, Reinhart C, Tran H, Kossmann K, Watzka M, and Oldenburg J (2013) Determination of the warfarin inhibition constant Ki for vitamin K 2,3-epoxide reductase complex subunit-1 (VKORC1) using an in vitro DTT-driven assay. *Biochim Biophys Acta* **1830:**4202-4210.

Bi YA, Lin J, Mathialagan S, Tylaska L, Callegari E, Rodrigues AD, and Varma MVS (2018) Role of Hepatic Organic Anion Transporter 2 in the Pharmacokinetics of R- and S-Warfarin: In Vitro Studies and Mechanistic Evaluation. *Mol Pharm* **15:**1284-1295.

Breckenridge A, Orme M, Wesseling H, Lewis RJ, and Gibbons R (1974) Pharmacokinetics and pharmacodynamics of the enantiomers of warfarin in man. *Clin Pharmacol Ther* **15:**424-430.

Burt T, Young G, Lee W, Kusuhara H, Langer O, Rowland M, and Sugiyama Y (2020) Phase 0/microdosing approaches: time for mainstream application in drug development? *Nat Rev Drug Discov* **19:**801-818.

Cheng S, Flora DR, Rettie AE, Brundage RC, and Tracy TS (2023) A Physiological-Based Pharmacokinetic Model Embedded with a Target-Mediated Drug Disposition Mechanism Can Characterize Single-Dose Warfarin Pharmacokinetic Profiles in Subjects with Various CYP2C9 Genotypes under Different Cotreatments. *Drug Metab Dispos* **51:**257-267.

Davies B and Morris T (1993) Physiological parameters in laboratory animals and humans. *Pharm Res* **10:**1093-1095.

Fidler M HM, Wilkins J, Wang W (2022) RxODE: Facilities for Simulating from ODE-Based Models. R package version 1.1.5.

Hazelett SE and Preusch PC (1988) Tissue distribution and warfarin sensitivity of vitamin K epoxide reductase. *Biochem Pharmacol* **37:**929-934.

Hignite C, Uetrecht J, Tschanz C, and Azarnoff D (1980) Kinetics of R andS warfarin enantiomers. *Clin Pharmacol Ther* **28:**99-105.

Kawai R, Mathew D, Tanaka C, and Rowland M (1998) Physiologically based pharmacokinetics of cyclosporine A: extension to tissue distribution kinetics in rats and scale-up to human. *J Pharmacol Exp Ther* **287:**457-468.

King SY, Joslin MA, Raudibaugh K, Pieniaszek HJ, Jr., and Benedek IH (1995) Dose-dependent pharmacokinetics of warfarin in healthy volunteers. *Pharm Res* **12:**1874-1877.

Koyama S, Toshimoto K, Lee W, Aoki Y, and Sugiyama Y (2021) Revisiting Nonlinear Bosentan Pharmacokinetics by Physiologically Based Pharmacokinetic Modeling: Target Binding, Albeit Not a Major Contributor to Nonlinearity, Can Offer Prediction of Target Occupancy. *Drug Metab Dispos* **49:**298-304.

Lappin G, Kuhnz W, Jochemsen R, Kneer J, Chaudhary A, Oosterhuis B, Drijfhout WJ, Rowland M, and Garner RC (2006) Use of microdosing to predict pharmacokinetics at the therapeutic dose: experience with 5 drugs. *Clin Pharmacol Ther* **80:**203-215.

Levy G (1994) Pharmacologic target-mediated drug disposition. *Clin Pharmacol Ther* **56:**248-252.

Levy G, Mager DE, Cheung WK, and Jusko WJ (2003) Comparative pharmacokinetics of coumarin anticoagulants L: Physiologic modeling of S-warfarin in rats and pharmacologic target-mediated warfarin disposition in man. *J Pharm Sci* **92:**985-994.

Lewis BC, Nair PC, Heran SS, Somogyi AA, Bowden JJ, Doogue MP, and Miners JO (2016) Warfarin resistance associated with genetic polymorphism of VKORC1: linking clinical response to molecular mechanism using computational modeling. *Pharmacogenet Genomics* **26:**44-50.

Mochizuki T, Aoki Y, Yoshikado T, Yoshida K, Lai Y, Hirabayashi H, Yamaura Y, Rockich K, Taskar K, Takashima T, Chu X, Zamek-Gliszczynski MJ, Mao J, Maeda K, Furihata K, Sugiyama Y, and Kusuhara H (2022) Physiologically-based pharmacokinetic model-based translation of OATP1B-mediated drug-drug interactions from coproporphyrin I to probe drugs. *Clin Transl Sci* **15:**1519-1531.

O'Reilly RA (1974) Studies on the optical enantiomorphs of warfarin in man. *Clin Pharmacol Ther* **16:**348-354.

Rodgers T and Rowland M (2006) Physiologically based pharmacokinetic modelling 2: predicting the tissue distribution of acids, very weak bases, neutrals and zwitterions. *J Pharm Sci* **95:**1238-1257.

Shaik AN, Grater R, Lulla M, Williams DA, Gan LL, Bohnert T, and LeDuc BW (2016) Comparison of enzyme kinetics of warfarin analyzed by LC-MS/MS QTrap and differential mobility spectrometry. *J Chromatogr B Analyt Technol Biomed Life Sci* **1008:**164-173.

Shen G, Cui W, Zhang H, Zhou F, Huang W, Liu Q, Yang Y, Li S, Bowman GR, Sadler JE, Gross ML, and Li W (2017) Warfarin traps human vitamin K epoxide reductase in an intermediate state during electron transfer. *Nat Struct Mol Biol* **24:**69-76.

Takada K and Levy G (1980) Comparative pharmacokinetics of coumarin anticoagulants XLIV: Dose-dependent pharmacokinetics of warfarin in rats. *J Pharm Sci* **69:**9-14.

Wu S, Chen X, Jin DY, Stafford DW, Pedersen LG, and Tie JK (2018) Warfarin and vitamin K epoxide reductase: a molecular accounting for observed inhibition. *Blood* **132:**647-657.

Yoshikado T, Aoki Y, Mochizuki T, Rodrigues A, Chiba K, Kusuhara H, and Sugiyama Y (2022) Cluster Gauss-Newton method analyses of PBPK model parameter combinations of coproporphyrin-I based on OATP1B-mediated rifampicin interaction studies. *CPT: Pharmacometrics Syst Pharmacol* **In press**.

Yoshikado T, Yoshida K, Kotani N, Nakada T, Asaumi R, Toshimoto K, Maeda K, Kusuhara H, and Sugiyama Y (2016) Quantitative Analyses of Hepatic OATP-Mediated Interactions Between Statins and Inhibitors Using PBPK Modeling With a Parameter Optimization Method. *Clin Pharmacol Ther* **100:**513-523.

Footnotes

Financial support for this research was provided by the international cooperation program managed by the National Research Foundation of Korea [NRF-2020K2A9A2A08000172] (to W.L.), Creative-Pioneering Researchers Program through Seoul National University (to W.L.), Grant-in-Aid for Scientific Research (B) [JP19H03392] (to Y.S.), and JSPS Bilateral Program [JPJSBP 120208820] (to Y.S.).

Conflict of Interest

No author has any potential conflict of interest to disclose.

DMD Fast Forward. Published on March 13, 2023 as DOI: 10.1124/dmd.122.000968
This article has not been copyedited and formatted. The final version may differ from this version.

Figure legends

Figure 1. Structure of the warfarin PBPK model incorporating saturable components for the hepatic active influx, metabolism, and target binding in the liver. Parameters are defined in the main text and Supplemental Material.

Figure 2. Blood PK (**A**) and TO (**B**) profiles of warfarin (racemic mixture) using the accepted parameter sets from the CGNM-based PBPK modeling of the warfarin blood PK data [2, 5, and 10 mg from (King et al., 1995) and 0.1 mg from (Lappin et al., 2006)] with the ODEs not separated for R- and S-warfarin. For each dose, open symbols represent the observed data, and lines represent the profiles with the accepted parameter sets. The accepted parameter sets (n=663) were used to draw the profiles, but the results were overlapping and appeared as a nearly single profile for each dose level.

Figure 3. Blood PK **(A)** and TO **(B)** profiles of warfarin using varying three-dose-level combinations: design A to D. For each dose (shown in different colors), open symbols represent the observed data, and lines represent the profiles with the accepted parameter sets. The accepted parameter sets were used to draw the profiles, but the results were overlapping and appeared as a nearly single profile for each dose level.

Figure 4. (A) Distribution of the accepted parameter sets from the CGNM runs using varying three-dose-level combinations: design A to D. The closed circles represent median values, and the dashed lines are drawn from the minimum to maximum values while the solid lines mark quartile values. The bandwidth represents kernel density estimated by Silverman's method. **(B)** Histograms for the bootstrap distribution of the accepted parameter sets from the CGNM runs using designs A to D.

Figure 5. Summary of the stereoselective PBPK-TO modeling (<RS #1, RS#2, and RS#3>) of R- and S-warfarin based on the warfarin blood PK data (0.1, 2, 5, and 10 mg racemic warfarin doses). (**A**) The <RS #1> incorporated the R- vs. S-warfarin differences in the hepatic metabolism and uptake processes but no differences in target interactions (K_d values kept the same for R- and S-warfarin). (**B** and **C**) While <RS#2>

DMD Fast Forward. Published on March 13, 2023 as DOI: 10.1124/dmd.122.000968
This article has not been copyedited and formatted. The final version may differ from this version.

assumed that K_d differences arise from the association process (i.e., $k_{on,S\text{-}warfarin}$ being three times to $k_{on,R\text{-}warfarin}$), <RS#3> assumed that K_d differences arise from the dissociation process (i.e., $k_{off,S\text{-}warfarin}$ being one-third to $k_{off,R\text{-}warfarin}$)**.** Blood PK and TO profiles of warfarin (separate profiles for S- and R-warfarin shown in purple and orange, respectively; combined profiles for both R- and S-warfarin shown in grey). For each dose, symbols represent the observed data, and lines represent the profiles with the accepted parameter sets, which appear to overlap.

Figure 6. (**A**) Parameters (CL/F and V_d/F) calculated via non-compartmental analysis of the observed blood PK profiles of warfarin [2, 5, and 10 mg from (King et al., 1995) and 0.1 mg from (Lappin et al., 2006)]. (**B**) A theoretical basis for the impact of dose selection on the apparent V_d for drugs that interact with targets of high affinity and abundance. Modeling-based analysis of the systemic PK data from low and intermediate doses (with varying levels of target saturation) can provide valuable information ascertaining the ratio of X_{TotalR}/K_d, thereby reducing uncertainty in the estimation of target binding parameters.

DMD Fast Forward. Published on March 13, 2023 as DOI: 10.1124/dmd.122.000968
This article has not been copyedited and formatted. The final version may differ from this version.

Table 1. List of ***optimized*** and ***fixed*** parameters in the warfarin PBPK model with the ordinary differential equations of no stereoisomeric separation. For parameter optimization by the Cluster Gauss-Newton Method (CGNM), the initial estimates were set with the upper and lower ranges as specified from 10^{-2} and 10^{2}-fold to the base values from the literature.

Parameter		Value/ range (min, max)	Calculation	Reference
K_d (nM)	Opt*	(0.041, 410)	Base value of 4.1 nM; 321 nM (as the total warfarin in plasma) x 0.013 ($f_{u,p}$)	Target-binding-related parameters from (Levy et al., 2003)
k_{off} (/h)	Opt	(0.000405, 4.05)	Base value of 0.0405 /h	
X_{TotalR} (μmol)	Opt	(0.117, 1,170)	Base value of 11.7 μmol; 0.167 μmole/kg x 70 kg	
$V_{max(met)}$ (μmol/h)	Opt	(0.08511, 851.1)	Base value of 8.511 μmol/h; the intrinsic metabolic clearance of (R) 0.4145 and (S) 1.288 L/h divided by the assumed $K_{m(met)}$ value (10 μM)	Hepatic metabolism and uptake parameters from (Bi et al., 2018)
$V_{max(act,inf)}$ (μmol/h)	Opt	(30.63, 306,300)	Base value of 3,063 μmol/h; averaged from (R) 4,067 μmol/h and (S) 2,059 μmol/h	
k_a (/h)	Opt	(0.1, 6)	upper bound as the gastric emptying rate of 0.1 min^{-1} (= 6 h^{-1})	(Levy et al., 2003)
$V_{central}$ (L)	Fixed	5.215	0.0745 L/kg x 70 kg	(Levy et al., 2003)
$K_{m(act,inf)}$ (μM)	Fixed	8.85	8.85 μM; averaged from (R) 10.4 μM and (S) 7.3 μM	(Bi et al., 2018)
R_{dif} ($PS_{dif,inf}$/ $PS_{act,inf}$)	Fixed	0.0355	$PS_{dif,inf}$ of 12.0 L/h; averaged from (R) 13.4 L/h and (S) 10.6 L/h $PS_{act,inf}$ of 337 L/h; averaged from (R) 391 L/h and (S) 282 L/h	(Bi et al., 2018)
$K_{m(met)}$ (μM)	Fixed	10	Assumed based on the reported K_m values	(Shaik et al., 2016)
$f_{u,B}$	Fixed	0.022	$f_{u,p}$ / R_b = 0.013/0.59	(Bi et al., 2018)
f_h	Fixed	0.69		
K_{pa}	Fixed	0.0883	*In silico* prediction	(Rodgers and Rowland, 2006)
K_{pm}	Fixed	0.115	*In silico* prediction	
K_{ps}	Fixed	0.477	*In silico* prediction	
Q_h (L/h)	Fixed	86.8	1.24 L/h/kg x 70 kg	(Davies and Morris, 1993)
Q_a (L/h)	Fixed	15.6	0.223 L/h/kg x 70 kg	
Q_m (L/h)	Fixed	44.9	0.642 L/h/kg x 70 kg	
Q_s (L/h)	Fixed	18.0	0.257 L/h/kg x 70 kg	
V_h (L)	Fixed	1.22	0.0174 L/kg x 70 kg	
V_a (L)	Fixed	10.0	0.143 L/kg x 70 kg	
V_m (L)	Fixed	30.0	0.429 L/kg x 70 kg	
V_s (L)	Fixed	7.77	0.111 L/h/kg x 70 kg	
V_{he} (L)	Fixed	0.469	0.0067 L/kg x 70 kg	(Kawai et al., 1998)

* Optimized; $f_{u,B}$, Fraction unbound in blood; $f_{u,p}$, Fraction unbound in plasma; R_b, Blood-to-plasma ratio; f_h, Fraction unbound in hepatocytes; Definition of the rest of the parameters provided in the Supplemental Material.

Table 2. List of ***optimized*** and ***fixed*** parameters in the stereoselective warfarin PBPK model with the ordinary differential equations of stereoisomeric separation. The parameters were kept same as Table 1, except for the stereoselective parameters listed below. Out of the six optimized parameters, the two parameters (X_{TotalR} and k_a) were assumed to be same between R- and S-warfarin.

Parameter		Value/ Range (lower, upper)	Description for stereoselective differences applied	Reference
$K_{m,(act,inf),R\text{-warfarin}}$ (μM)	Fixed	10.4	(Experimentally obtained values reported in the literature)	(Bi et al., 2018)
$K_{m,(act,inf),S\text{-warfarin}}$ (μM)	Fixed	7.3		
$R_{dif,R\text{-warfarin}}$ ($PS_{dif,inf,R\text{-warfarin}}$ / $PS_{act,inf,R\text{-warfarin}}$)	Fixed	0.0341	$PS_{dif,inf}$: (R) 13.4 L/h, (S) 10.6 L/h $PS_{act,inf}$: (R) 391 L/h, (S) 282 L/h	
$R_{dif,S\text{-warfarin}}$ ($PS_{dif,inf,S\text{-warfarin}}$ / $PS_{act,inf,S\text{-warfarin}}$)	Fixed	0.0374		
$V_{max(met),R\text{-warfarin}}$ (μmole/h)	Opt	(0.04145, 414.5)	Base value of 4.145 μmole/h $\mathbf{V_{max(met),S\text{-warfarin}} = V_{max(met),R\text{-warfarin}}}$ x **3.10** (The fold-difference of 3.10 based on the reported $V_{max(met)}$ values for (R) 0.1175 and (S) 0.365 μmol/min/mg microsomal protein)	(Bi et al., 2018)
$V_{max(act,inf),R\text{-warfarin}}$ (μmole/h)	Opt	(40.67, 406,700)	Base value of 4,067 μmole/h $\mathbf{V_{max(act,inf),S\text{-warfarin}} = V_{max(act,inf),R\text{-warfarin}}}$ x **0.506** (The fold-difference of 0.506 based on the reported values for (R) 335 and (S) 169.6 pmol/min/million hepatocytes)	
$K_{d,R\text{-warfarin}}$ (nM)	Opt	(0.041, 410)	The target affinity of S-warfarin assumed to be 3 times that of R-warfarin, based on the reported relationship between dose or concentration and response. The respective assumptions as summarized below.	(Breckenridge et al., 1974; O'Reilly, 1974; Hignite et al., 1980)
$k_{off,R\text{-warfarin}}$ (/h)	Opt	(0.000405, 4.05)		([a] k_{on} defined by k_{off}/K_d)

	R/S analysis scenario		
	<RS#1>	**<RS#2>**	**<RS#3>**
$\frac{K_{d,S-warfarin}}{K_{d,R-warfarin}}$	Unity (assumed same for R- and S-warfarin)	**1/3** (S-warfarin having one-third to R-warfarin)	
$\frac{k_{off,S-warfarin}}{k_{off,R-warfarin}}$		1	**1/3**
$\frac{k_{on,S-warfarin}{}^{a}}{k_{on,R-warfarin}{}^{a}}$		**3**	1

DMD Fast Forward. Published on March 13, 2023 as DOI: 10.1124/dmd.122.000968
This article has not been copyedited and formatted. The final version may differ from this version.

Table 3. Summary of the accepted parameters (n=663 sets, SSR ranging from 0.11526-0.11532, Rank 1 values in bold) for the CGNM run analyzing the blood PK data from all four warfarin dose levels with no stereoisomeric consideration (results shown in Figure 2) and additional secondary parameters calculated for metabolic clearance ($CL_{met,inf}$), permeability clearance ($PS_{act,inf}$), and overall intrinsic clearance ($CL_{int,all}$).

	Value			
	Rank 1	min	max	median
Optimized				
K_d (nM)	**6.30**	6.27	6.31	6.30
k_{off} (/h)	**0.0903**	0.0899	0.0906	0.0903
X_{TotalR} (μmole)	**4.26**	4.24	4.26	4.26
$V_{max(met)}$ (μmole/h)	**16.84**	16.82	16.85	16.84
$V_{max(act,inf)}$ (μmole/h)	**$2.76x10^{11}$**	$1.26x10^{6}$	$4.96x10^{16}$	$4.64x10^{10}$
k_a (/h)	**6.00**	5.92	6.00	6.00
Secondary (using 'rank 1' parameters)				
k_{on} (/h/μM)	**14.33**	14.28	14.39	14.33
$PS_{act,inf}$ (L/h)[a]	**$3.12x10^{10}$**	$1.42x10^{5}$	$5.61x10^{15}$	$5.25x10^{9}$
$CL_{met,int}$ (L/h)[b]	**1.68**	1.68	1.69	1.68
$CL_{int,all}$ (L/h)[c]	**11.93**	11.91	11.94	11.93

[a] $PS_{act,inf}$, calculated as $V_{max\ (act,inf)}/K_{m\ (act,inf)}$;
[b] $CL_{met,int}$, calculated as $V_{max(met)}/K_{m(met)}$;
[c] $CL_{int,all}$, calculated based on the extended clearance concept model,

$$CL_{int,\,all} = \left(PS_{dif,inf} + PS_{act,inf}\right) \cdot \frac{CL_{met,int}}{PS_{dif,eff} + CL_{met,int}} \quad \text{Eq. (*1)}$$

$PS_{dif,inf}$, calculated as $PS_{act,inf}$ x R_{dif} and R_{dif} assumed to be 0.0355 based on the literature (Bi et al., 2018);
$PS_{dif,eff}$, calculated as $PS_{dif,inf}$ / 0.243 (γ value for anions as reported previously) (Yoshikado et al., 2016)

Considering the values of $CL_{met,int}$ (1.7 L/h), R_{dif} (0.0355), and $PS_{act,inf}$ (>105 L/h), the value of $PS_{dif,eff}$ would become considerably larger than that of $CL_{met,int}$, simplifying Eq.(*1) as follows:

$$CL_{\text{int,all}} = CL_{met,int} \cdot \frac{\left(PS_{dif,inf} + PS_{act,inf}\right)}{PS_{dif,eff}} = CL_{met,int} \cdot \frac{\left(PS_{dif,inf} + PS_{act,inf}\right)}{PS_{dif,inf}/\gamma} = CL_{met,int} \cdot \gamma \cdot \left(1 + \frac{PS_{act,inf}}{PS_{dif,inf}}\right) \quad \text{Eq. (*2)}$$

Table 4. Summary of the accepted parameters (Rank 1 values in bold; minimum, maximum, and median values in parentheses) for the CGNM runs using the blood PK data from all four warfarin dose levels (ALL) or varying three-dose level designs (Designs A-D) and additional secondary parameters calculated for metabolic clearance ($CL_{met,inf}$), permeability clearance ($PS_{act,inf}$), and overall intrinsic clearance ($CL_{int,all}$).

		ALL dataset	Design			
			A	B	C	D
Warfarin racemic doses (mg)		**0.1, 2, 5, 10**	**2, 5, 10**	**0.1, 5, 10**	**0.1, 2, 5**	**0.1, 2, 10**
# of datapoints		36	36	36	36	36
# of accepted parameter sets		663	586	469	641	645
SSR ranges	(min, max)	(0.11526, 0.11532)	(0.0564, 0.0565)	(0.0991, 0.0992)	(0.0822, 0.0822)	(0.0820, 0.0820)
Optimized						
K_d (nM)	**Rank 1**	**6.30**	**6.22**	**5.60**	**6.42**	**6.38**
	(min, max; median)	(6.27, 6.31; 6.30)	(6.13, 6.31; 6.22)	(5.57, 5.66; 5.60)	(6.42, 6.43; 6.42)	(6.37, 6.39; 6.38)
k_{off} (/h)	**Rank 1**	**0.0903**	**0.0432**	**0.0961**	**0.0932**	**0.0901**
	(min, max; median)	(0.0899, 0.0906; 0.0903)	(0.0425, 0.0449; 0.0432)	(0.0956, 0.0971; 0.0961)	(0.0931, 0.0932; 0.0931)	(0.0898, 0.0902; 0.0901)
X_{TotalR} (µmole)	**Rank 1**	**4.26**	**4.45**	**3.75**	**4.24**	**4.34**
	(min, max; median)	(4.24, 4.26; 4.26)	(4.44, 4.47; 4.45)	(3.74, 3.77; 3.75)	(4.24, 4.25; 4.24)	(4.33, 4.34; 4.34)
$V_{max(met)}$ (µmole/h)	**Rank 1**	**16.84**	**16.51**	**16.95**	**17.78**	**16.28**
	(min, max; median)	(16.82, 16.85; 16.84)	(16.46, 16.57; 16.51)	(16.90, 16.96; 16.94)	(17.77, 17.79; 17.78)	(16.26, 16.28; 16.28)
$V_{max(act,inf)}$ (µmole/h)	**Rank 1**	**$2.75x10^{11}$**	**$2.83x10^{8}$**	**$4.23x10^{9}$**	**$4.65x10^{10}$**	**$1.87x10^{9}$**
	(min, max; median)	($1.26x10^{6}$, $4.96x10^{16}$; $4.64x10^{10}$)	($2.51x10^{4}$, $2.49x10^{11}$; $5.17x10^{6}$)	($3.85x10^{5}$, $2.78x10^{16}$; $4.45x10^{9}$)	($5.02x10^{7}$, $9.44x10^{15}$; $3.43x10^{10}$)	($2.53x10^{7}$, $5.16x10^{16}$; $2.38x10^{10}$)
k_a (/h)	**Rank 1**	**6.00**	**5.58**	**6.00**	**6.00**	**6.00**
	(min, max; median)	(5.92, 6.00; 6.00)	(5.19, 6.00; 5.58)	(5.94, 6.00; 6.00)	(6.00, 6.00; 6.00)	(6.00, 6.00; 6.00)
Secondary (using 'rank 1' parameters)						
k_{on} (/h/µM)		14.3	6.94	17.2	14.5	14.1
$PS_{act,inf}$ (L/h)		$3.12x10^{10}$	$3.19x10^{7}$	$4.78x10^{8}$	$5.26x10^{9}$	$2.11x10^{8}$
$CL_{met,int}$ (L/h)		1.68	1.65	1.69	1.78	1.63
$CL_{int,all}$ (L/h)		11.93	11.70	12.01	12.60	11.54

Table 5. Summary of the CGNM runs <RS#1-#3> analyzing all four warfarin dose levels with stereoselective considerations applied (as described in Table 2): the accepted parameters (Rank 1 values in bold; minimum, maximum, and median values in parentheses) and additional secondary parameters calculated for metabolic clearance ($CL_{met,inf}$), permeability clearance ($PS_{act,inf}$), and overall intrinsic clearance ($CL_{int,all}$).

		RS#1 (n=361; SSR 0.101885-0.102854)		RS#2 (n=333; SSR 0.109241-0.109241)		RS#3 (n=357; SSR 0.108873-0.11102)	
		R-warfarin	S-warfarin	R-warfarin	S-warfarin	R-warfarin	S-warfarin
Optimized							
K_d (nM)	**Rank 1**	**6.03**		**8.94**	**2.98**	**9.00**	**3.00**
	(min, max; median)	(5.93, 6.13; 6.03)		(8.93, 8.94; 8.94)	($K_{d,R-warfarin}$x1/3)	(8.80, 9.16; 9.00)	($K_{d,R-warfarin}$x1/3)
k_{off} (/h)	**Rank 1**	**0.095**		**0.0858**		**0.141**	**0.047**
	(min, max; median)	(0.094, 0.102; 0.0095)		(0.0893, 0.0894; 0.0894) (Same for R- and S-warfarin)		(0.137, 0.159; 0.141)	($k_{off,R-warfarin}$x1/3)
X_{TotalR} (µmole)	**Rank 1**	**3.96**		**3.98**		**3.94**	
	(min, max; median)	(3.90, 4.02; 3.96)		(3.98, 3.98; 3.98)		(3.87, 4.01; 3.94)	
$V_{max(met)}$ (µmole/h)	**Rank 1**	**9.9**	**30.69**	**10.5**	**32.55**	**10.5**	**32.55**
	(min, max; median)	(9.8, 10.0; 9.9)	($V_{max(met),R-warfarin}$ x3.10)	(10.5, 10.5; 10.5)	($V_{max(met),R-warfarin}$ x3.10)	(10.4, 10.6; 10.5)	($V_{max(met),R-warfarin}$ x3.10)
$V_{max(act,inf)}$ (µmole/h)	**Rank 1**	**$4.72x10^{11}$**	**$2.39x10^{11}$**	**$6.16x10^{13}$**	**$3.12x10^{13}$**	**$6.77x10^{10}$**	**$3.43x10^{10}$**
	(min, max; median)	($8.19x10^4$, $5.02x10^{15}$; $6.08x10^9$)	($V_{max(act,inf),R-warfarin}$ x0.506)	($6.50x10^8$, $2.66x10^{16}$; $8.94x10^{10}$)	($V_{max(act,inf),R-warfarin}$ x0.506)	($4.20x10^4$, $3.22x10^{16}$; $4.52x10^9$)	($V_{max(act,inf),R-warfarin}$ x0.506)
k_a (/h)	**Rank 1**	**6.00**		**6.00**		**6.00**	
	(min, max; median)	(5.25, 6.00; 6.00)		(6.00, 6.00; 6.00)		(4.83, 6.00; 6.00)	
Secondary (using 'rank 1' parameters)							
k_{on} (/h/µM)		15.8		9.60	28.8	15.7 (Same for R- and S-warfarin)	
$PS_{act,inf}$ (L/h)		$4.54x10^{10}$	$3.27x10^{12}$	$5.92x10^{12}$	$4.27x10^{12}$	$6.51x10^9$	$4.69x10^9$
$CL_{met,int}$ (L/h)		0.99	3.07	1.05	3.25	1.05	3.26
$CL_{int,all}$ (L/h)		7.29	20.7	7.73	21.9	7.76	22.0

Figure 1

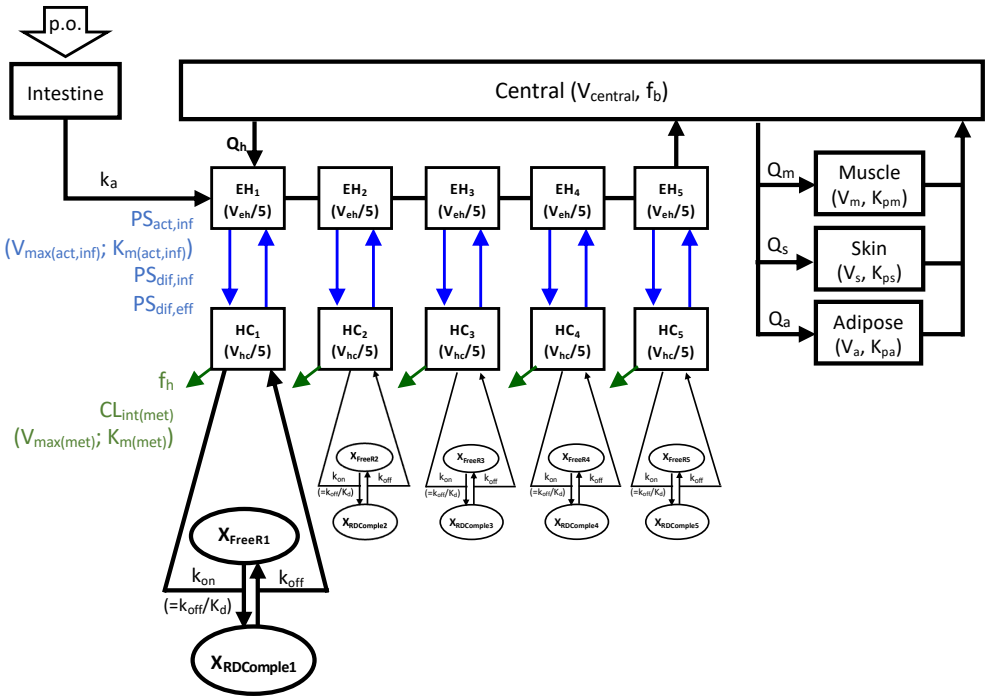

Figure 2

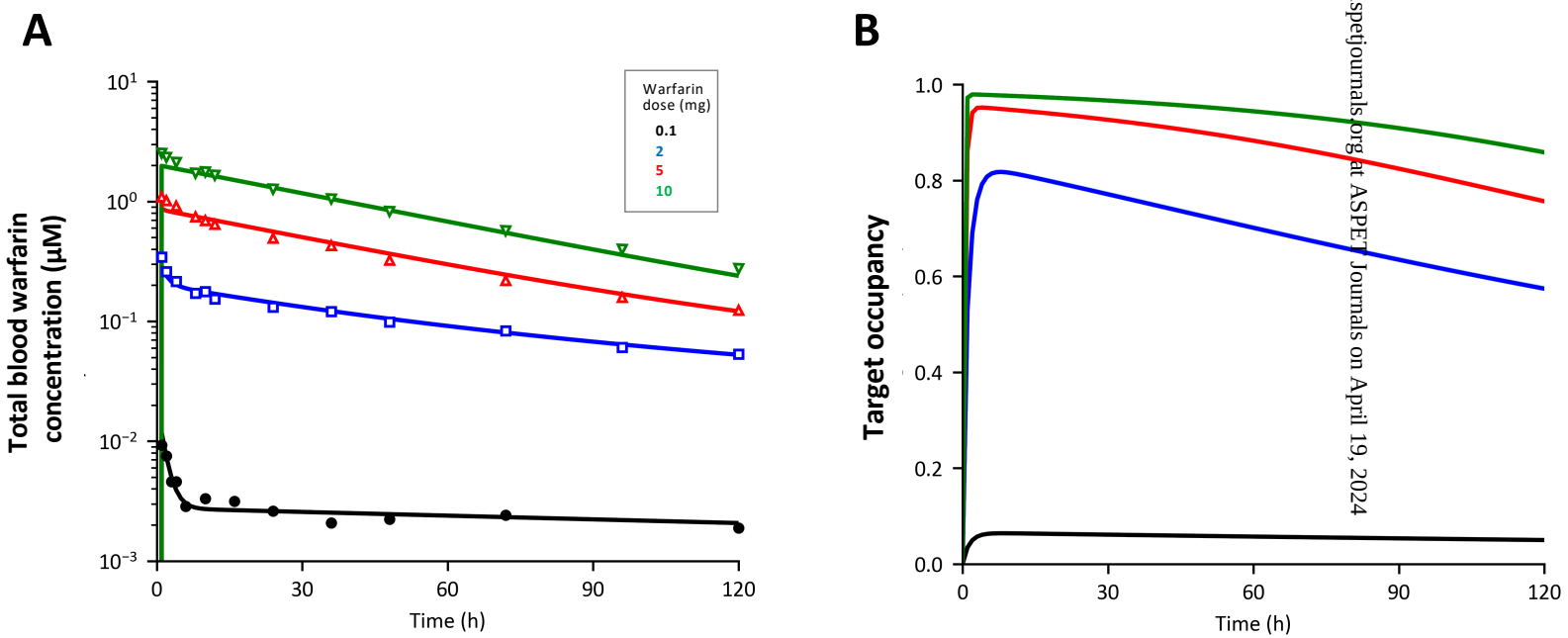

Figure 3

	ALL	Design			
		A	B	C	D
doses (mg)	0.1, 2, 5, 10	2, 5, 10	0.1, 5, 10	0.1, 2, 5	0.1, 2, 10

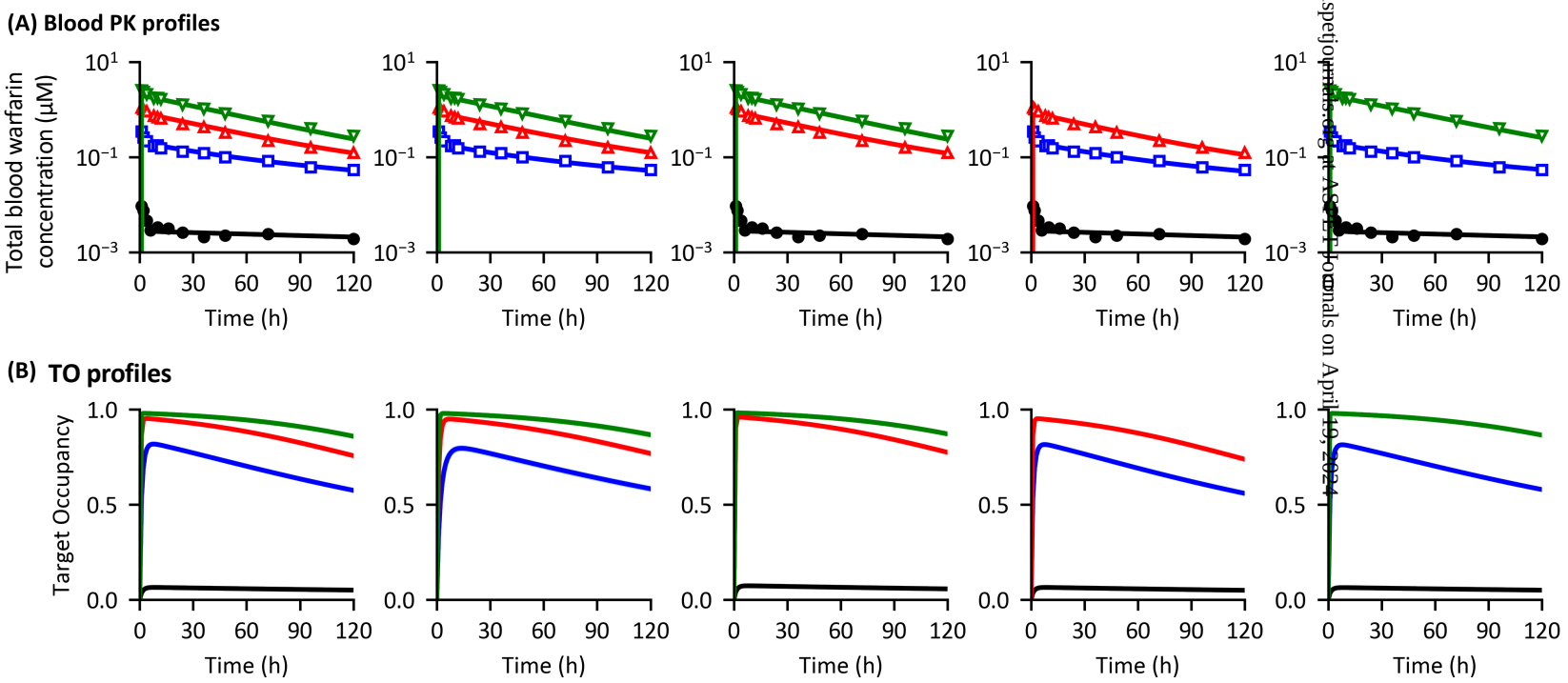

Figure 4

(A) Distribution of the initial and accepted parameter sets

	doses (mg)
ALL	0.1, 2, 5, 10
A	2, 5, 10
B	0.1, 5, 10
C	0.1, 2, 5
D	0.1, 2, 10

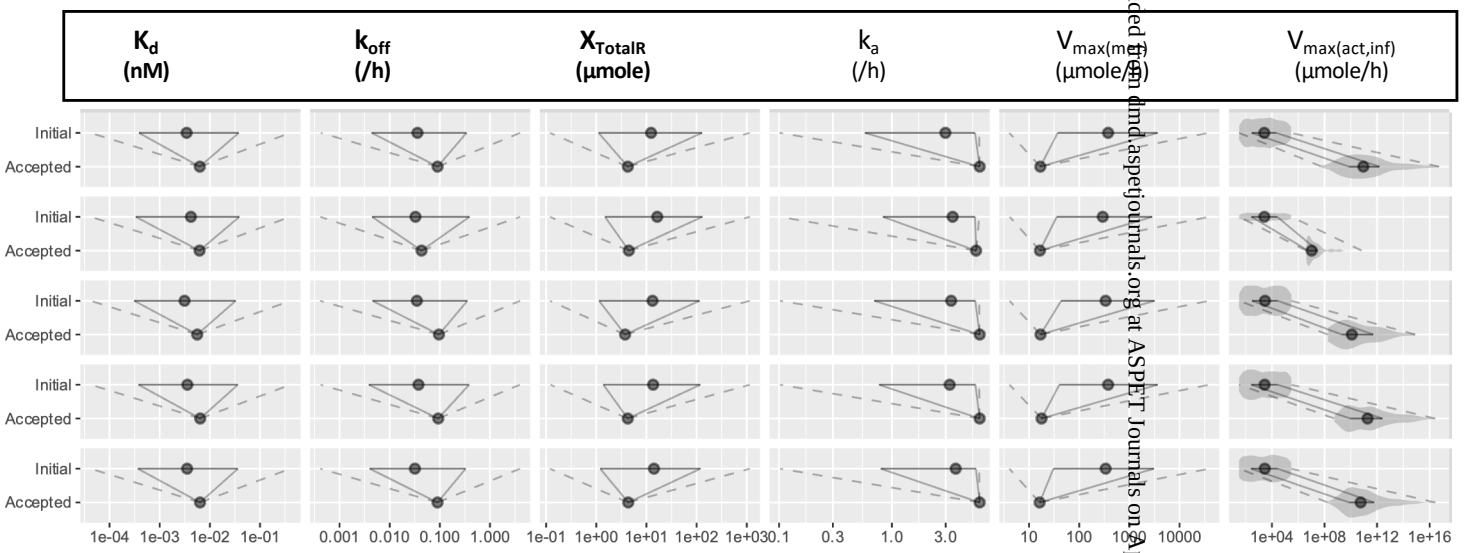

(B) Bootstrap distribution

	doses (mg)
ALL	0.1, 2, 5, 10
A	2, 5, 10
B	0.1, 5, 10
C	0.1, 2, 5
D	0.1, 2, 10

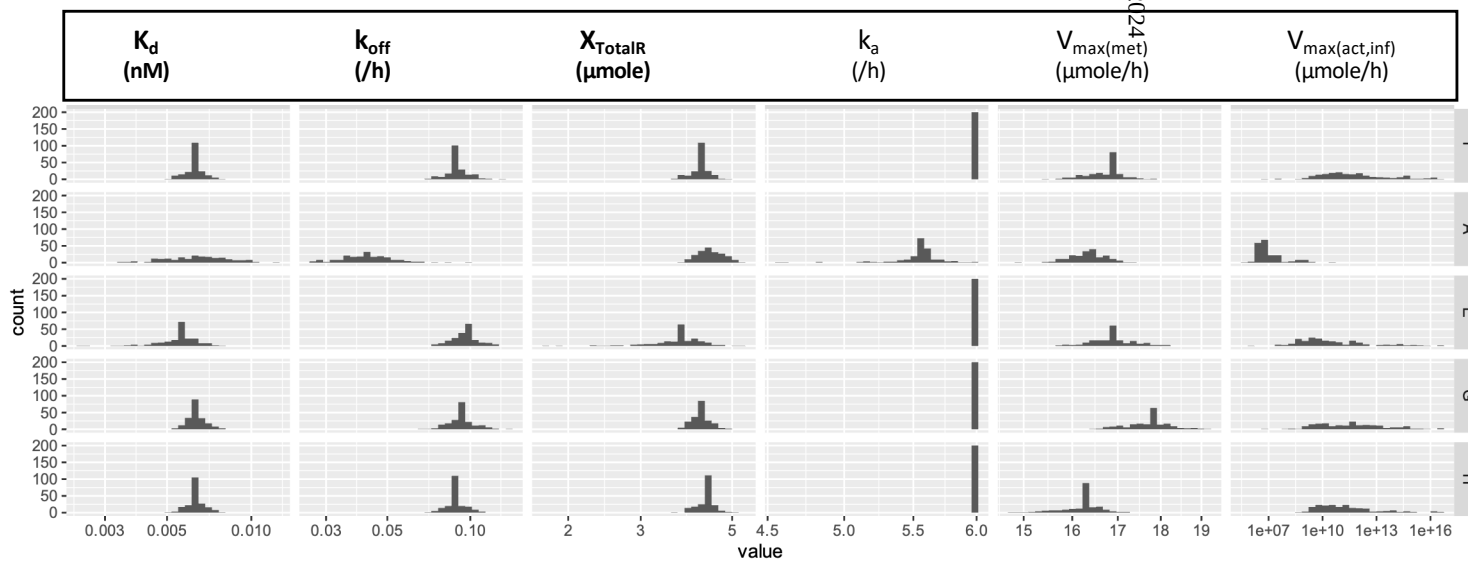

Figure 5

	$\frac{K_{d,S-warfarin}}{K_{d,R-warfarin}}$	$\frac{k_{off,S-warfarin}}{k_{off,R-warfarin}}$	$\frac{k_{on,S-warfarin}}{k_{on,R-warfarin}}$	Blood PK and TO profiles
(A) **RS#1**	1	1	1	Blood PK / TO 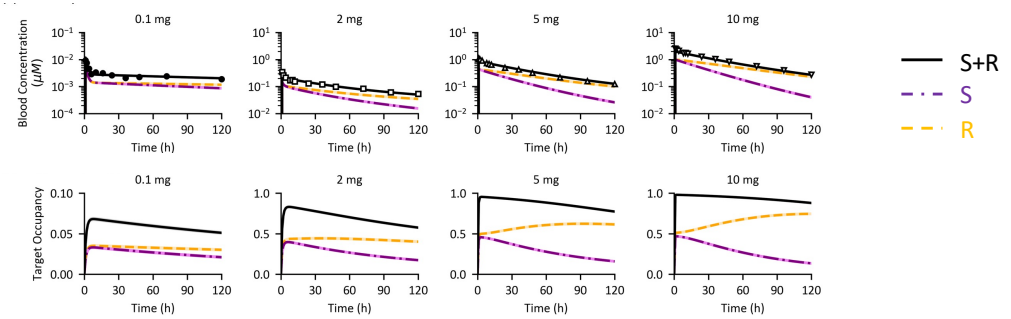
(B) **RS#2**	1/3	1	**3** Differences at the association step	Blood PK / TO 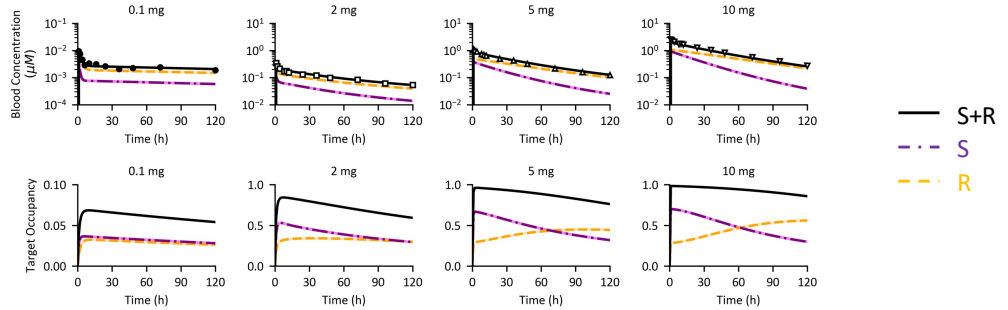
(C) **RS#3**	1/3	**1/3** Differences at the dissociation step	1	Blood PK / TO 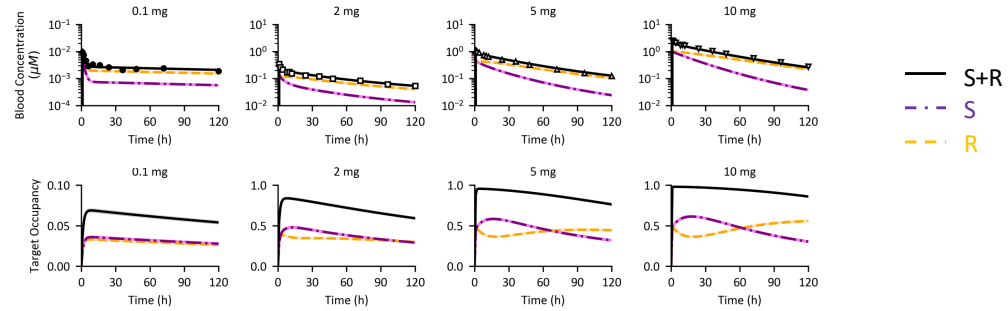

Figure 6

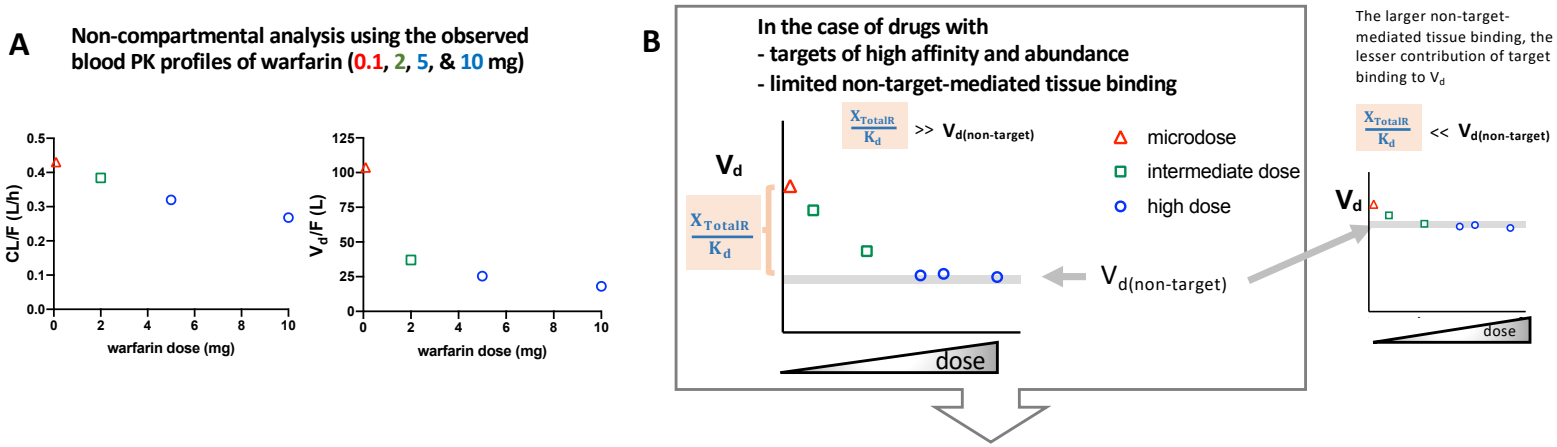
A
Non-compartmental analysis using the observed blood PK profiles of warfarin (0.1, 2, 5, & 10 mg)
CL/F (L/h)
warfarin dose (mg)
Vd/F (L)
warfarin dose (mg)
B
In the case of drugs with
- targets of high affinity and abundance
- limited non-target-mediated tissue binding
Vd
>> Vd(non-target)
microdose
intermediate dose
high dose
Vd(non-target)
dose
The larger non-target-mediated tissue binding, the lesser contribution of target binding to Vd
<< Vd(non-target)
Vd
dose
Dose-scending PK studies in preclinical animals (at microdose, intermediate & high doses) may verify the occurrence of TMDD & identify target binding parameters *in vivo*

Supplemental Figure

Predicting *in vivo* Target Occupancy (TO) Profiles via PBPK-TO Modeling of Warfarin Pharmacokinetics in Blood: Importance of Low Dose Data and Prediction of Stereoselective Target Interactions

Wooin Lee, Min-Soo Kim, Jiyoung Kim, Yasunori Aoki, Yuichi Sugiyama

Figure S1. Simulated PK and TO profiles of R- and S-warfarin in subjects receiving repeated warfarin dosing (10 mg for 2 days and 3 mg afterwards) using the rank 1 parameter set of the CGNM run <RS#2>

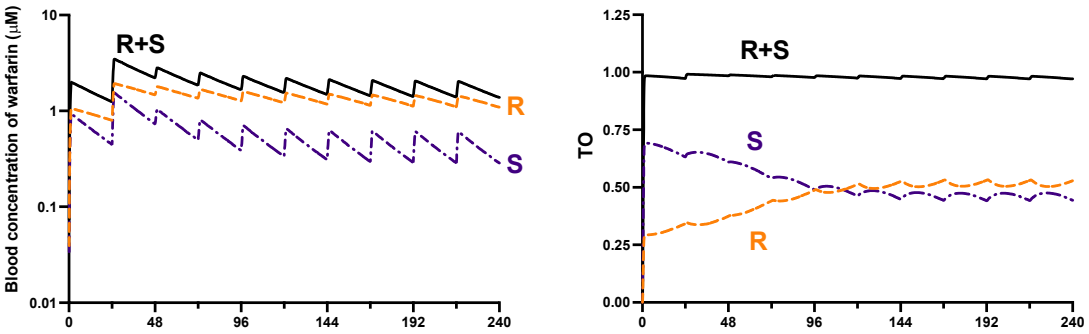

Supplemental Material

Predicting *in vivo* Target Occupancy (TO) Profiles via PBPK-TO Modeling of Warfarin Pharmacokinetics in Blood: Importance of Low Dose Data and Prediction of Stereoselective Target Interactions

Wooin Lee, Min-Soo Kim, Jiyoung Kim, Yasunori Aoki, Yuichi Sugiyama

Table S1. Summary of the accepted parameters (rank 1, maximum, minimum, and median values) for the CGNM repeat runs #1 and #2 analyzing all four warfarin dose levels and additional secondary parameters calculated for metabolic clearance ($CL_{met,inf}$), permeability clearance ($PS_{act,inf}$), and overall intrinsic clearance ($CL_{int,all}$).

	Repeat run #1 (N=678 sets; SSR, 0.11527-0.11527)				**Repeat run #2** (N=659 sets; SSR, 0.11526-0.11538)			
	Rank 1	min	max	median	**Rank 1**	min	max	median
Optimized								
K_d (nM)	**6.30**	6.28	6.31	6.30	**6.30**	6.26	6.33	6.30
k_{off} (/h)	**0.090**	0.090	0.090	0.090	**0.090**	0.090	0.091	0.090
X_{TotalR} (µmole)	**4.26**	4.25	4.26	4.26	**4.26**	4.25	4.28	4.26
$V_{max(met)}$ (µmole/h)	**16.84**	16.83	16.84	16.84	**16.84**	16.81	16.86	16.84
$V_{max(act,inf)}$ (µmole/h)	**$3.31*10^{8}$**	$2.43*10^{7}$	$2.14*10^{16}$	$3.43*10^{10}$	**$1.63*10^{14}$**	$5.82*10^{5}$	$2.99*10^{16}$	$2.43*10^{10}$
k_a (/h)	**6.00**	6.00	6.00	6.00	**6.00**	5.86	6.00	6.00
Secondary (using 'rank 1' parameters)								
k_{on} (/h/µM)	**14.33**	14.26	14.37	14.33	**14.33**	14.21	14.40	14.33
$PS_{act,inf}$ (L/h)	**$3.73*10^{7}$**	$2.75*10^{6}$	$2.41*10^{15}$	$3.88*10^{9}$	**$1.84*10^{13}$**	$6.58*10^{4}$	$3.38*10^{15}$	$2.74*10^{9}$
$CL_{met,int}$ (L/h)	**1.68**	1.68	1.69	1.68	**1.68**	1.68	1.69	1.68
$CL_{int,all}$ (L/h)	**11.93**	11.93	11.94	11.93	**11.93**	11.92	11.95	11.93

$PS_{act,inf}$, calculated as $V_{max\ (act,inf)}/K_{m\ (act,inf)}$; $PS_{dif,inf}$, calculated as $PS_{act,inf}$ x R_{dif} and R_{dif} assumed to be 0.0355 based on the literature (Bi et al. 2018);

$PS_{dif,eff}$, calculated as $PS_{dif,inf}$ / 0.243 (γ value for anions as reported previously) (Yoshikado et al., 2016);

$CL_{met,int}$, calculated as $V_{max(met)}/K_{m(met)}$;

$CL_{int,all}$, calculated based on the extended clearance concept model,

$$CL_{int,\,all} = \left(PS_{dif,inf} + PS_{act,inf}\right) \cdot \frac{CL_{met,int}}{PS_{dif,eff} + CL_{met,int}} = \left(1.0355 \cdot PS_{act,inf}\right) \cdot \frac{CL_{met,int}}{PS_{act,inf} \cdot \frac{0.0355}{0.243} + CL_{met,int}}$$

Supplemental Equations

Nomenclature/Abbreviations

C, the total concentration of the drug; $C_{central}$, the drug concentration in the central compartment; $C_{EH(i)\ (i=1\text{-}5)}$, the drug concentration in the i^{th} hepatic extracellular compartment; $C_{HC(i)\ (i=1\text{-}5)}$, the drug concentration in the i^{th} hepatocellular compartment; $C_{adipose}$, C_{muscle}, and C_{skin}, the drug concentration in the adipose, the muscle, and the skin compartments, respectively; $V_{central}$, V_{eh}, and V_{hc}, the volume of the central compartment, the hepatic extracellular compartment, and the hepatocellular compartment, respectively; V_a, V_m, and V_s, the volume of the adipose, the muscle, and the skin compartment, respectively; Q_h, Q_m, Q_s, and Q_a, the blood flow rate to the liver, the muscle, the skin, and the adipose, respectively; $K_{m,act,inf}$ and $V_{max,act,inf}$, the Michaelis-Menten constant and the maximum velocity for the active influx through the basolateral membrane of hepatocytes; $K_{m(met)}$, $V_{max(met)}$, the Michaelis-Menten constant and the maximum velocity for the hepatic metabolism; $f_{u,B}$ and f_h, the fraction of the unbound drug in blood, and in the hepatocellular compartment, respectively; R_{dif}, the ratio of the influx intrinsic clearance via passive diffusion across the sinusoidal membrane of hepatocytes ($PS_{dif,inf}$) to the influx intrinsic clearance via active uptake across the sinusoidal membrane of hepatocytes ($PS_{act,inf}$); $PS_{dif,eff}$, the efflux intrinsic clearance via passive diffusion across the sinusoidal membrane of hepatocytes, calculated as $PS_{dif,inf}/\gamma$ ($\gamma = 0.243$ for anions); k_a, the absorption rate constant; k_{off} and k_{on}, the dissociation and association rate constant of the drug to the target, respectively; $K_d = k_{off}/k_{on}$, the dissociation equilibrium constant of the drug to the target; K_{pa}, adipose-to-blood drug concentration ratio; K_{pm}, muscle-to-blood drug concentration ratio; K_{ps}, skin-to-blood drug concentration ratio; R_b, blood to plasma drug concentration ratio; TO, the ratio of target occupancy; X_a, the amount of the drug absorbed; X_{TotalR}, the total amount of the target receptor assumed to be equally divided into the five serially placed hepatocellular compartments; $X_{FreeR(i)}$ (i=1-5) and $X_{RDcomplex(i)}$ (i=1-5), the amount of the unoccupied (free) target receptor and the target receptor-drug complex in the i^{th} hepatocellular compartment, respectively.

[Intestine]

$$\frac{dX_a}{dt} = -k_a \cdot X_a$$ (The bioavailability was assumed to be unity based on the previous report, Bi et al. (2018))

[Central compartment]

$$V_{central} \cdot \frac{dC_{central}}{dt} = Q_h(C_{EH5} - C_{central}) - Q_m\left(C_{central} - \frac{C_{muscle}}{K_{pm}}\right) - Q_s\left(C_{central} - \frac{C_{skin}}{K_{ps}}\right) - Q_a\left(C_{central} - \frac{C_{adipose}}{K_{pa}}\right)$$

[Liver]

Hepatic extracellular compartment [EH(1) to EH(5)]

For EH(1),

$$\frac{V_{eh}}{5} \cdot \frac{dC_{EH(1)}}{dt} = k_a \cdot X_a + Q_h \cdot \left(C_{central} - C_{EH(1)}\right) - \frac{0.2 \cdot V_{max(act,inf)} \cdot f_{u,B} \cdot C_{EH(1)}}{K_{m(act,inf)} + f_{u,B} \cdot C_{EH(1)}} - \frac{0.2 \cdot V_{max(act,inf)} \cdot R_{dif}}{K_{m(act,inf)}} \cdot f_{u,B} \cdot C_{EH(1)}$$
$$+ \frac{0.2 \cdot V_{max(act,inf)} \cdot \frac{R_{dif}}{0.243}}{K_{m(act,inf)}} \cdot f_h \cdot C_{HC(1)}$$

For EH(i), i=2-5,

$$\frac{V_{eh}}{5}\cdot\frac{dC_{EH(i)}}{dt}=Q_h\cdot\left(C_{EH(i-1)}-C_{EH(i)}\right)-\frac{0.2\cdot V_{max(act,inf)}\cdot f_{u,B}\cdot C_{EH(i)}}{K_{m(act,inf)}+f_{u,B}\cdot C_{EH(i)}}-\frac{0.2\cdot V_{max(act,inf)}\cdot R_{dif}}{K_{m(act,inf)}}\cdot f_{u,B}\cdot C_{EH(i)}$$
$$+\frac{0.2\cdot V_{max(act,inf)}\cdot\frac{R_{dif}}{0.243}}{K_{m(act,inf)}}\cdot f_h\cdot C_{HC(i)}$$

Hepatocellular compartment [HC(1) to HC(5)]

For HC(i), i=1-5,

$$\frac{V_{hc}}{5}\cdot\frac{dC_{HC(i)}}{dt}=\frac{0.2\cdot V_{max(act,inf)}\cdot f_{u,B}\cdot C_{EH(i)}}{K_{m(act,inf)}+f_{u,B}\cdot C_{EH(i)}}+\frac{0.2\cdot V_{max(act,inf)}\cdot R_{dif}}{K_{m(act,inf)}}\cdot f_{u,B}\cdot C_{EH(i)}-\frac{0.2\cdot V_{max(act,inf)}\cdot\frac{R_{dif}}{0.243}}{K_{m(act,inf)}}\cdot f_h\cdot C_{HC(i)}$$
$$-\frac{0.2\cdot V_{max(met)}\cdot f_h\cdot C_{HC(i)}}{K_{m(met)}+f_h\cdot C_{HC(i)}}-\frac{k_{off}}{K_d}\cdot f_h\cdot C_{HC(i)}\cdot X_{FreeR(i)}+k_{off}\cdot X_{RDComplex(i)}$$

[Distribution compartments (muscle, adipose, and skin)]

$$V_m\cdot\frac{dC_{muscle}}{dt}=Q_m(C_{central}-\frac{C_{muscle}}{K_{pm}})$$

$$V_a\cdot\frac{dC_{adipose}}{dt}=Q_a(C_{central}-\frac{C_{adipose}}{K_{pa}})$$

$$V_s\cdot\frac{dC_{skin}}{dt}=Q_s(C_{central}-\frac{C_{skin}}{K_{ps}})$$

[Target binding]

For i = 1-5,

$$\frac{dX_{FreeR(i)}}{dt}=k_{off}\cdot X_{RDComplex(i)}-\frac{k_{off}}{K_d}\cdot f_h\cdot C_{HC(i)}\cdot X_{FreeR(i)}$$

$$\frac{dX_{RDcomplex(i)}}{dt}=\frac{k_{off}}{K_d}\cdot f_h\cdot C_{HC(i)}\cdot X_{FreeR(i)}-k_{off}\cdot X_{RDcomplex(i)}$$

$$\frac{dRO}{dt}=\frac{1}{X_{TotalR}}\{\frac{k_{off}}{K_d}\cdot f_h\left(C_{HC(1)}\cdot X_{FreeR(1)}+C_{HC(2)}\cdot X_{FreeR(2)}+C_{HC(3)}\cdot X_{FreeR(3)}+C_{HC(4)}\cdot X_{FreeR(4)}+C_{HC(5)}\cdot X_{FreeR(5)}\right)$$
$$-k_{off}\left(X_{RDcomplex(1)}+X_{RDcomplex(2)}+X_{RDcomplex(3)}+X_{RDcomplex(4)}+X_{RDcomplex(5)}\right)\}$$

Other equations

$$PS_{dif,inf}=R_{dif}\cdot PS_{act,inf}$$

$$PS_{dif,eff}=PS_{dif,inf}/\gamma$$

$$CL_{met,int}=V_{max(met)}/K_{m(met)}$$

$$CL_{int,\,all}=\left(PS_{dif,inf}+PS_{act,inf}\right)\cdot\frac{CL_{met,int}}{PS_{dif,eff}+CL_{met,int}}$$

For the analysis <RS#1-3>, the equations were duplicated and separated for R- and S-warfarin except for the following equations considering competitive interactions of S- and R-warfarin for the free target;

For i=1-5,

$$\frac{dX_{FreeR(i)}}{dt} = k_{off} \cdot (X_{RDcomplex(i),R-warfarin} + X_{RDcomplex(i),S-warfarin}) - \frac{k_{off}}{K_d} \cdot f_h \cdot (C_{HC(i),R-warfarin} + C_{HC(i),S-warfarin}) \cdot X_{FreeR(i)}$$